# Formation mechanism of the protective layer in a blast furnace hearth

*Ke-xin Jiao*[1,2], *Jian-liang Zhang*[1,2], *Zheng-jian Liu*[1,2], *Meng Xu*[3], *and Feng Liu*[1,2]

1) School of Metallurgical and Ecological Engineering, University of Science and Technology Beijing, Beijing 100083, China

2) State Key Laboratory of Advanced Metallurgy, University of Science and Technology Beijing, Beijing 100083, China

3) Shougang Research Institute of Technology, Beijing 100043, China

**Abstract:** A variety of techniques, such as chemical analysis, scanning electron microscopy–energy dispersive spectroscopy, and X-ray diffraction, were applied to characterize the adhesion protective layer formed below the blast furnace taphole level when a certain amount of titanium-bearing burden was used. Samples of the protective layer were extracted to identify the chemical composition, phase assemblage, and distribution. Furthermore, the formation mechanism of the protective layer was determined after clarifying the source of each component. Finally, a technical strategy was proposed for achieving a stable protective layer in the hearth. The results show that the protective layer mainly exists in a bilayer form in the sidewall, namely, a titanium-bearing layer and a graphite layer. Both the layers contain the slag phase whose major crystalline phase is magnesium melilite ($Ca_2MgSi_2O_7$) and the main source of the slag phase is coke ash. It is clearly determined that solid particles such as graphite, Ti(C,N) and $MgAl_2O_4$ play an important role in the formation of the protective layer, and the key factor for promoting the formation of a stable protective layer is reasonable control of the evolution behavior of coke.

**Keywords:** blast furnaces; hearths; protective layers; electrochemical corrosion

## 1. Introduction

The campaign life of a blast furnace is heavily dependent upon the lifespan of the hearth. Generally speaking, the protective layer that develops between the hot face of the refractory lining and the liquid iron must be given special attention so as to prevent erosion due to the direct contact of the hot face with the liquid iron. Moreover, it is of vital importance to determine the formation mechanism of this protective layer, which plays a key role in extending the campaign life of a blast furnace [1–4].

Past research has typically concentrated on the wear mechanism of the hearth and bottom lining. Given specific raw materials and fuels, the wear involving the penetration of hot metal into the carbon bricks and the erosion resulting from dissolution caused by carburization has been extensively investigated. Relevant experimental studies on the mechanical wear have shown that the wear of the refractory lining in the hearth is caused by hot metal erosion owing to the peripheral flow and chemical attack from alkali, zinc oxides, molten slag, and iron. Moreover, oxide gases such as $CO_2$ and $H_2O$ are responsible for the damage sustained by the carbon bricks. It is noteworthy that the employment of high quality carbon bricks is capable of prolonging the service life of the blast furnace hearth and bottom [5–7].

On the other hand, past research on the protective layer of the hearth has mainly focused on the formation of titanium carbonitride Ti(C,N). It has already been proven that the melting point of Ti(C,N) precipitating in the hearth and gradually evolving into a sticky material is quite high. Ti(C,N) solid particles readily precipitate near the cooling area, particularly when the refractory lining in the hearth is seriously eroded [8–9]. Consequently, the hearth is well protected. However, studies relevant to the formation mechanism of the intricate protective layer formed in the hearth are quite rare, and, a great controversy on the source of the slag phase still exists below the taphole level. Some researchers hold the opinion that the slag phase is derived from the blast furnace slag, whereas others argue that the slag phase is preexisting below the taphole level during the

Ⓐ Springer

normal production process in the blast furnace [10–11].

In the present study, the protective layer formed below the taphole level of a blast furnace in operation for approximately 18 months was sampled to analyze the main chemical composition, distribution, deposition behavior, and mineral transformation mechanisms using chemical analysis, X-ray diffraction (XRD), and scanning electron microscopy–energy dispersive spectroscopy (SEM-EDS). A useful guide is proposed for the practical and controlled formation of a stable protective layer in a blast furnace hearth during the normal production process.

## 2. Experimental

### 2.1. Investigation of the damage sustained by a blast furnace hearth

The working volume of the studied blast furnace was 1200 m$^3$. The furnace bottom was lined with GL65 high alumina bricks as well as carbon bricks, whereas for the hearth sidewall, only GL65 high alumina bricks were used. The blast furnace was commissioned on September 9, 2011, and shut down on March 9, 2013. Investigations of the erosion of the hearth refractory lining during repair of the blast furnace illustrated the occurrence of abnormal erosion to the hearth (elephant foot) and pan bottom. The local remaining thickness of the weakest area in the hearth was 80–150 mm. In addition, the alumina bricks lining were severely eroded and the remaining thickness was only 475 mm (the total thickness of the 3-layer alumina brick lining was 3 × 345 mm = 1035 mm). In contrast, the carbon bricks in the bottom were nearly free from erosion. The hearth bottom erosion profile is shown in Fig. 1.
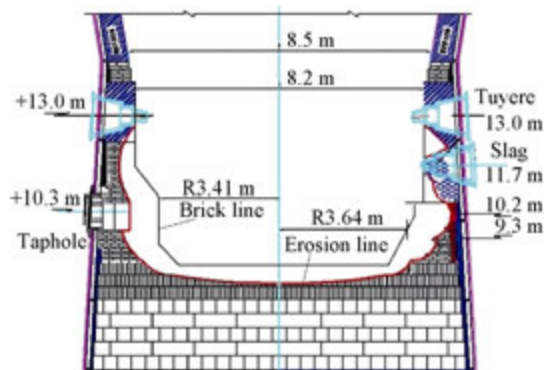


**Fig. 1.    Erosion profile of the blast furnace hearth bottom.**

### 2.2. Protective layer sample

It can be observed from Fig. 1 that most of the hearth lining was insignificantly eroded, and the thickness of the refractory lining was generally in the range of 400–800 mm.

However, the erosion in the vicinity of the taphole, especially below the taphole, was relatively serious. In this research, the protective layer was sampled 1 m below the taphole level (height of 9.3 m in Fig. 1) where the adhesive materials attached to the refractory were found. It is noted that during sampling, this scab was retained in its original shape to the greatest extent possible.

### 2.3. Experimental installation

The chemical composition, phase assemblage, and microstructure of the sampled protective layer were analyzed via XRF (Shimadzu XRF-1800, Japan), XRD (Shimadzu XRD-1800, Japan), and SEM-EDS (JEOL JMS-5600-lv, Japan). In addition, a phase diagram for the protective layer was calculated by Factsage (Thermochemical Database System) software.

## 3. Results and discussion

### 3.1. Chemical composition analysis of the protective layer

The chemical composition of the protective layer is listed in Table 1. The carbon content in the protective layer was quite high, and accounted for 13.25wt% of the sample. In addition, the protective layer contained a large concentration of titanium compounds, upwards of 52.91wt%. The slag phase consisted of CaO, MgO, $Al_2O_3$, $SiO_2$, and MnO, and, among these components, the CaO content was the highest. In addition, it was readily determined that the binary basicity was 1.2.

**Table 1.    Chemical composition of the protective layer in the blast furnace hearth**                                                    wt%

| C | T.Fe | CaO | MgO | $SiO_2$ | $Al_2O_3$ | MnO | S | $TiO_2$ |
|---|------|-----|-----|---------|-----------|-----|---|---------|
| 13.25 | 9.05 | 18.52 | 4.28 | 15.32 | 8.10 | 1.90 | 0.70 | 52.91 |

Note: T.Fe means total Fe.

### 3.2. SEM-EDS analysis of the protective layer

Fig. 2 shows the results of SEM observation and EDS analyses of the hearth sample. As shown in the figure, the protective layer is mainly composed of iron (point A of Fig. 2(a)), slag (point B), and titanium compounds (point C). At elevated temperature in the hearth, both the slag phase and the molten iron are liquid, whereas the titanium compounds remain in a solid state. These solid particles of various sizes are surrounded by the molten slag as well as the liquid iron, and, thus, effectively increase the viscosity of the liquid phases. As a result, the protective layer is formed along the hearth sidewall, and direct contact between the hot metal and the refractory lining is avoided.
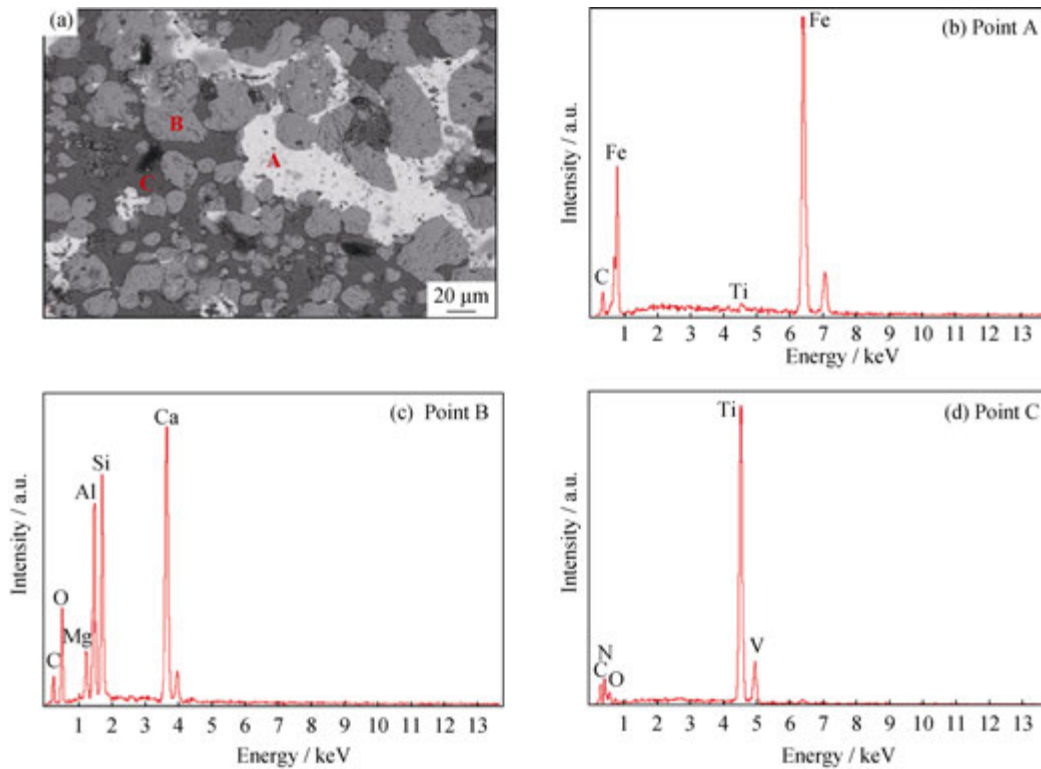
**Fig. 2.  SEM image (a) and EDS spectra (b–d) concerning the protective layer near the refractory lining.**

Fig. 3 provides a more expansive view of the structure of the protective layer. An obvious layered structure is readily observed as follows: (1) a homogeneous mixing layer consisting of slag, iron, and titanium compounds whose thickness is 2 mm lies against the side of the refractory; (2) next to the mixing layer, a slag phase distributed in a random pattern along with a small quantity of iron embedded in the carbon matrix is seen.
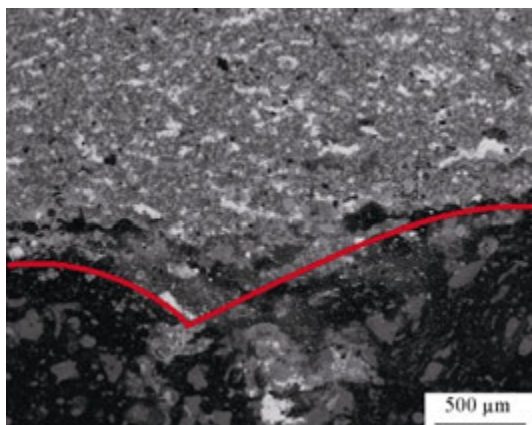


**Fig. 3.  Low-magnification SEM image of the protective layer near the refractory lining.**

### 3.3. XRD analysis of the protective layer

To identify the phase assemblage of the protective layer,

XRD analysis was performed on the sample and the result is shown in Fig. 4. The major crystalline phases in the protective layer are Fe, TiO, $Fe_{0.95}Ti_{0.25}$, $TiC_{0.7}N_{0.3}$, $Ca_2MgSi_2O_7$, $MgAl_2O_4$, $Ca_8Mg_2Al_3Si_7O_{28}$, and graphite. Combined with the SEM-EDS analysis in Fig. 2, it is concluded that the main form of titanium compound observed in the protective layer is $TiC_{0.7}N_{0.3}$. In addition, the slag phase in the protective layer consists mainly of magnesium melilite ($Ca_2MgSi_2O_7$).
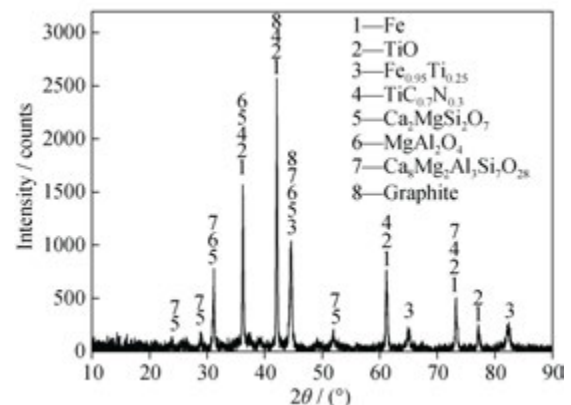


**Fig. 4.  XRD spectrum of the protective layer near the refractory lining.**

As demonstrated from EDS analysis in Fig. 2, a large amount of carbon is contained in the protective layer. To determine the degree of graphitization of the carbon, the in-

1020

*Int. J. Miner. Metall. Mater., Vol. 22, No. 10, Oct. 2015*

terplanar spacing $d_{(002)}$ of the polycrystalline carbon observed in Fig. 4 was used. The carbon stacking height $L_c$ increases with decreasing $d_{(002)}$, and, consequently, indicates an increasing degree of graphitization. The interplanar spacing $d_{(002)}$ was calculated via the Bragg equation, as given by Eq. (1) [12]:

$$d = \frac{n\lambda}{2\sin\theta} \qquad (1)$$

where $\theta$ is the incidence angle of the X-ray beam, and $\lambda$ is the X-ray wavelength. The variable $\lambda$ is the wavelength of incident X-ray beams and $n$ is an integer.

The degree of graphitization of carbon $\rho$ was calculated according to the spacing $d_{(002)}$, as given by Eq. (2) [13]:

$$\rho = \frac{d_{max} - d_{(002)}}{d_{max} - d_{min}} \qquad (2)$$

where $d_{max}$ refers to the maximum interplanar spacing (0.43 nm) and $d_{min}$ is the minimum interplanar spacing (0.3354 nm). In addition, the spacing $d_{(002)}$, as measured by XRD, was 0.43 nm.

Accordingly, the calculated degree of carbon graphitization of the protective layer was about 0.994. Therefore, the carbon in the protective layer existed in the form of graphitic carbon.

### 3.4. Analysis of the protective layer formation mechanism

3.4.1. Analysis of the formation process of the protective layer

During the normal production process, the density of the molten slag in the blast furnace hearth is about 2.5 g/cm$^3$, whereas the density of the hot metal is around 7.0 g/cm$^3$, which is considerably higher than that of molten slag [14]. Therefore, owing to the buoyancy of the liquid iron, it is difficult to form a slag shell below the taphole level, and, the greater the depth of the iron layer, the more difficult it is to form a slag shell at that depth. However, because the hearth functions in a non-stationary state, blast furnace slag may dip below the taphole level due to the combined influence of the iron siphonage, the outlet gas flow, and hot metal circulation. On the other hand, the very large density variation existing between the hot metal and liquid slag severely limits the deposit of liquid slag at the level where the elephant foot was formed. Therefore, the blast furnace slag is not particularly important with respect to the formation of the protective layer that protects the key parts of the hearth.

From SEM-EDS analyses, Ti(C,N), iron, and slag were found in the protective layer. Iron was the main phase below

the taphole level, and Ti(C,N) was determined to exist in the key parts of the hearth adhering to the refractory hot face, rather than being left behind after the tapping process.

Moreover, the slag phase and Ti(C,N) were mixed together. Therefore, during the normal production of the blast furnace, the presence of the slag phase was confirmed in the lower area of the furnace hearth such as the secondary cooling stave.

The deadman in the hearth tends to float and sink continuously due to the fluctuations of the molten slag and the hot metal accumulated in the hearth and the change of gas flow in the raceway. Therefore, it is quite likely for the deadman to sink into the hearth deeply. Consequently, the coke filled in the hearth might closely contact with the hot face of the refractory lining. With the coke dissolved into the liquid iron through carburization, erosion of the carbon bricks proceeds continuously. In addition, the residual ash serves as the source of the slag phase below the taphole level. The detailed evolution process is illustrated in Fig. 5. It is worth noting that the elements such as C and N which are expressed in the form of [C] and [N] in Fig. 5 are those dissolved into the liquid iron.
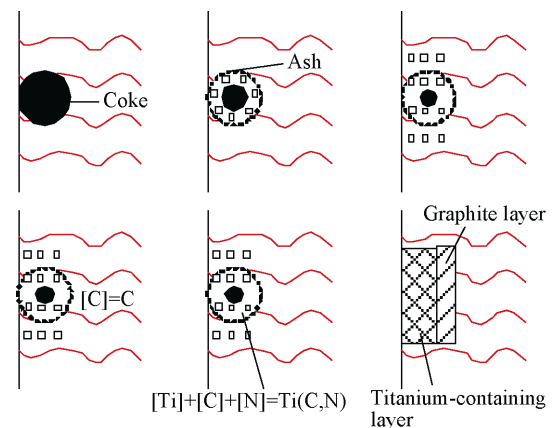


**Fig. 5. Schematic representation of the evolutionary process that forms the protective layer.**

With the coke being dissolved into the liquid iron continuously [15], a small part of the coke ash adheres to the surface of the coke while the remaining remains in the slag phase. However, due to the circulation of the hot metal, the coke ash has a tendency to adhere to the refractory lining surface. Generally speaking, there were two types of ash. One is the slag phase capable of diffusing from the coke particle surface to the refractory surface with a certain fluidity formed at high temperatures. The other was the unmelted phase with a high melting point that adheres to the refractory surface during the flow of the hot metal.

The viscosity of the hot metal at 1773 K is about $5.0 \times 10^{-3}$ Pa·s. In contrast, the viscosity of the slag is about 0.3 Pa·s, which is about 60 times larger than that of the hot metal [16]. Therefore, at the refractory lining surface, the viscosity of the hot metal containing the slag phase increases dramatically. Meanwhile, the hot metal near the refractory lining flows slowly, and a relatively large thermal resistance layer is formed so that the surface temperature of the refractory is reduced. At this temperature, carbon dissolved into the hot metal precipitates in the form of graphitic carbon. Under the condition of protecting the blast furnace with titanium, a certain amount of titanium would be contained in the hot metal. Thereby, the dissolved titanium is able to promote the precipitation of graphitic carbon and form Ti(C,N) because the binding capacity of titanium with iron is greater than that of carbon with iron. The chemical reaction formulas are given as Eqs. (3)–(5) [17−18].

$$[C] = C_{graphite}, \quad \Delta G_C^{\ominus} = 22590 - 42.26T \quad (3)$$

$$[Ti] + [C] = TiC(s), \quad \Delta G_{TiC}^{\ominus} = -176934 + 100.11T \quad (4)$$

$$[Ti] + [N] = TiN(s), \quad \Delta G_{TiN}^{\ominus} = -291000 + 107.91T \quad (5)$$
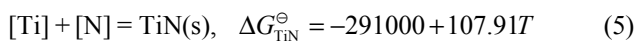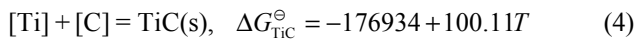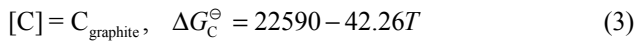
Thermodynamic calculations indicate that [C] (the carbon dissolved in the hot metal) is more likely to combine with dissolved components [Ti] and [N] in the form of Ti(C,N), precipitating in the presence of titanium in the hot metal. Therefore, on the hot face of the refractory, a titanium-bearing layer would preferentially form. In addition, the thermal resistance of the titanium-bearing layer increases with increasing thickness. As a consequence, the temperature of the titanium-bearing layer in the liquid iron boundary increases; thus, precipitation in the form of Ti(C,N) is weakened until a relatively stable state is achieved. Moreover, the heat transfer of the hearth as well as the temperature variation between the hearth thermocouple and cooling water is reduced. At this point, titanium ore loses its usual ability to protect the hearth. However, in normal blast furnace operation, the thickness of the formed titanium-bearing layer decreases owing to the washing and penetration of the hot metal. Therefore, the temperature at the interface between the hot metal and the titanium-bearing layer drops. Finally, [C] precipitates in the form of graphite attaching to the surface of the titanium-bearing layer until achieving a state of dynamic balance in the liquid iron.

### 3.4.2. Analysis of the evolution of the slag phase in the protective layer

As shown in Table 2, the chemical composition of the coke used in the blast furnace is obviously different from that of the protective layer (Table 1). It can be observed that the main components of coke ash are $Al_2O_3$ and $SiO_2$, whereas the CaO content is low, so that it is difficult to form the slag phase of the protective layer.

**Table 2. Chemical composition of coke**    wt%

| C | Ash | | | | | Volatile | $H_2O$ |
| | CaO | MgO | $Al_2O_3$ | $SiO_2$ | $Fe_2O_3$ | | |
|---|---|---|---|---|---|---|---|
| 87.5 | 1.62 | 0.68 | 27.86 | 59.06 | 6.32 | 0.6 | 0.6 |

However, the coke ash is involved with a series of physical and chemical reactions because of the high temperature in the hearth. The carbon in the coke is responsible for reducing the content of oxides in the ash. For the scab at the boundary of the hot face, the precipitated graphite capable of reacting with the ash possesses very high activity. Fig. 6 shows SEM-EDS results of the protective layer in the hearth. It is observed that the $SiO_2$ in the ash is reduced to Si. The chemical reactions are given by Eqs. (6) and (7):

$$SiO_2 + C = SiO + CO, \quad \Delta G^{\ominus} = 686134 - 329.61T \quad (6)$$

$$SiO + C = Si + CO, \quad \Delta G^{\ominus} = -126275 - 1.393T \quad (7)$$
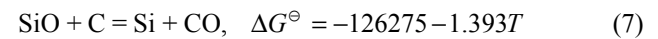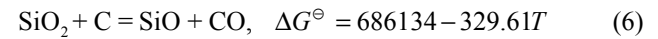
It is noteworthy that the generated Si existing in the form of solid particles diffuses into the carbon matrix.

The content of $SiO_2$ and $Al_2O_3$ in the coke ash is greatly reduced; thus, $Fe_2O_3$ is easily reduced. As a result, the proportion of CaO increases as well as that of MgO. In addition, the change of the coke ash content leads to the formation of the magnesium aluminum spinel phase derived from the reaction between MgO and $Al_2O_3$, which is suggested by the SEM-EDS data provided in Fig. 7. Moreover, XRD patterns also indicate the existence of the magnesium aluminum spinel phase in the protective layer. On the one hand, it is expected that the content of CaO in the residual ash would increases significantly due to the formation of the magnesium aluminate spinel phase. On the other hand, the viscosity of the molten slag would be increased and the adhesive ability of the protective layer improved remarkably.

For the chemical composition in the protective layer, the MgO content accounted for 10wt%. With the proportion of MgO fixed, the quaternary phase diagram of the $CaO$–$MgO$–$SiO_2$–$Al_2O_3$ system was calculated via Factsage software, which is shown in Fig. 8. The straight line labeled 1 in the figure represents the slag basicity, which is 1.2, and the straight line labeled 2 represents the $Al_2O_3$ content, which was 17.5wt% in the protective layer. The intersection point of the two lines is the melilite region, which was the main component of the protective layer. Under the condition of a constant content of alkalinity, the

melilite phase would gradually evolve into the magnesium melilite phase as the $Al_2O_3$ phase content was reduced. The key point, which is the intersection of lines 1 and 3, indicates an $Al_2O_3$ content of 12.9wt%, and the melting temperature of melilite is 1684 K. Therefore, in the formation process of the protective layer, $Al_2O_3$ would be combined with MgO partially to form the magnesium aluminate spinel phase, and, consequently, the $Al_2O_3$ content would be lowered while the content of CaO relatively improved.

Based on the above-mentioned analysis, it is concluded that the main source of the protective layer was coke ash. This indicates that the $Al_2O_3$ content in the coke ash should be reduced as much as possible to effectively promote the reduction of $SiO_2$. In addition, a relatively high content of CaO should be maintained. Only through these measures can the coke ash transform into the magnesium melilite phase to form a viscous layer for protecting the hearth.

3.4.3. Formation mechanism of the Al phase in the protective layer

A large amount of Al was observed in the protective layer, as shown in Fig. 9. At high temperatures, the generated Al is a liquid and congregates in the protective layer. Moreover, it is difficult for $Al_2O_3$ to react with C. The formation mechanism of Al was analyzed as follows.
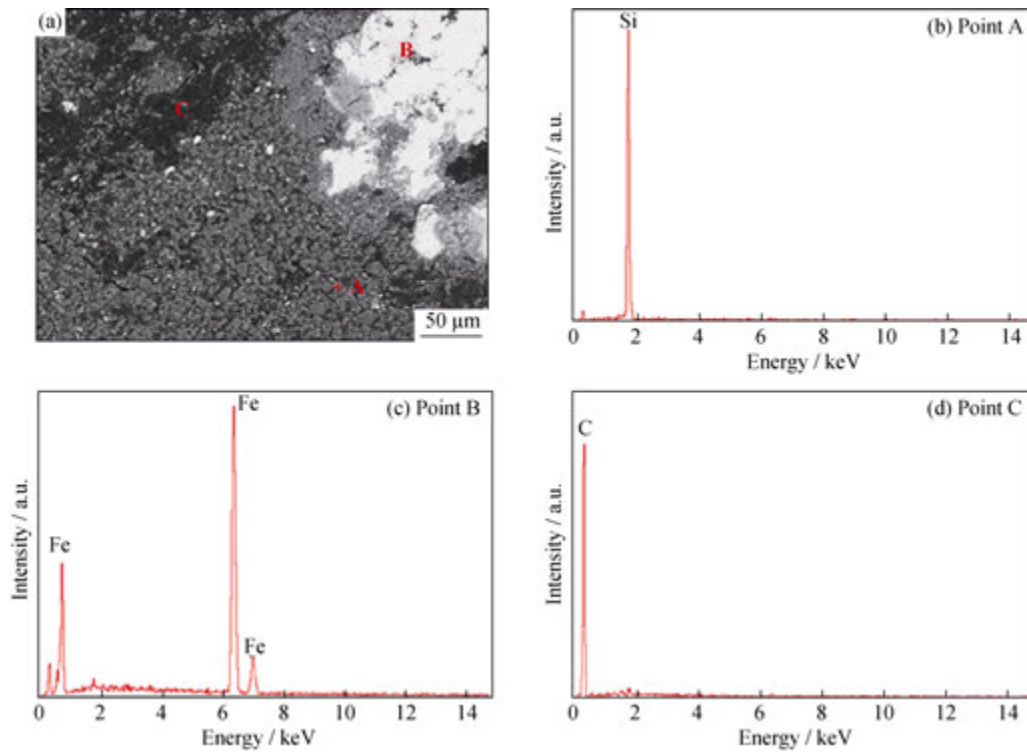


Fig. 6.    SEM image (a) and EDS (b−d) spectra regarding silicon reduction in the protective layer.
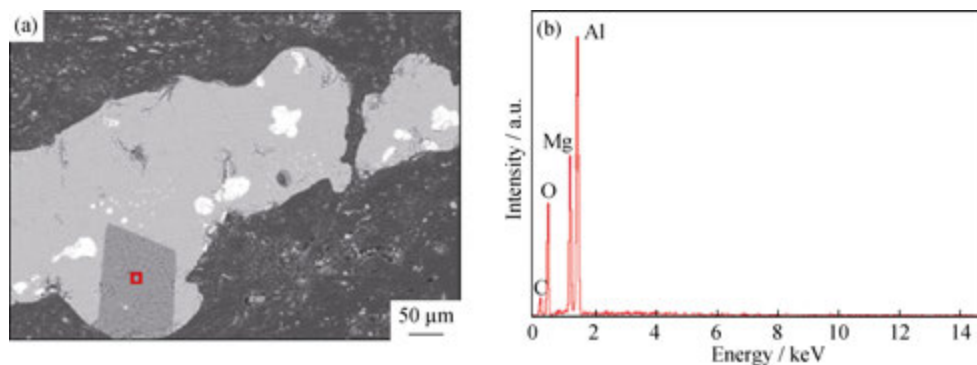


Fig. 7.    SEM image (a) and EDS spectrum (b) indicative of the magnesium aluminate spinel phase generated in the protective layer.
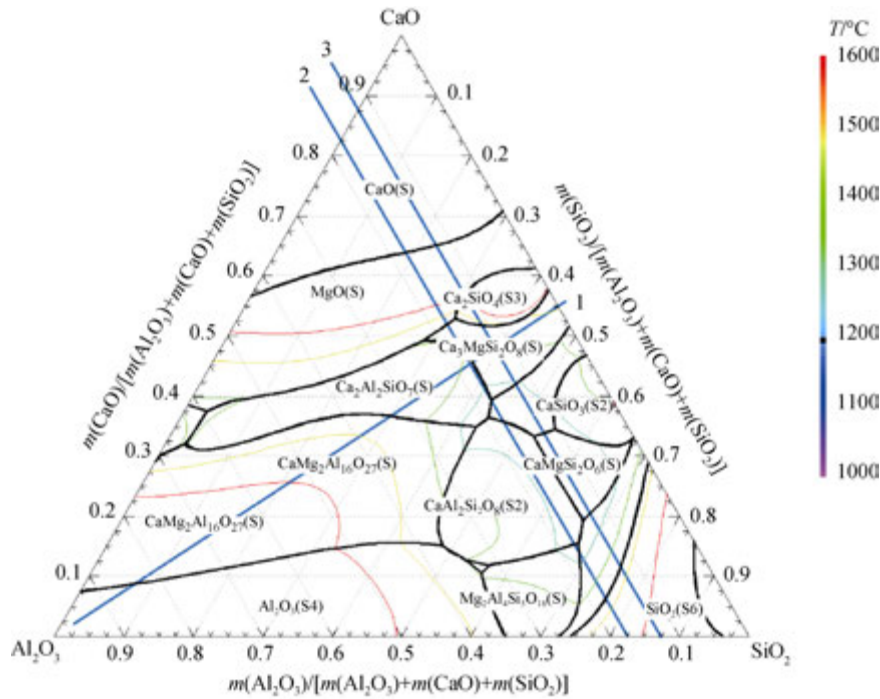
**Fig. 8.   Quaternary phase diagram of the CaO–MgO–SiO₂–Al₂O₃ system with the MgO content accounted for 10wt%.**
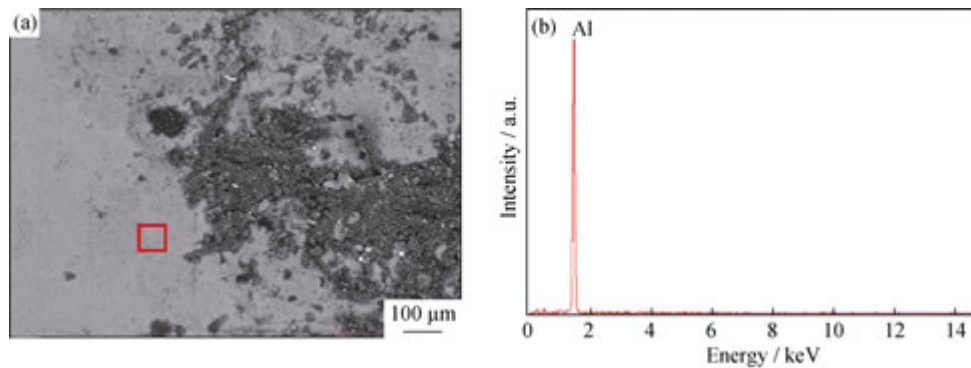


**Fig. 9.   SEM image (a) and EDS spectrum (b) of aluminum reduced in the protective layer.**

In the presence of slag between the high-temperature liquid iron and the refractory lining, slag acts as an ion conductor, which is a type of electrolyte with good conductive performance. Carbon is also a good electrical conductor. Thus, a cell can be composed at the corrosion interface [19]:

Refractory | Slag | Molten iron.

The electrochemical reactions due to the electrochemical corrosion of the refractory can be given as follows.

Cathodic reaction:

$$3[C] = 3C^{2+} + 6e^- \qquad (8)$$

Anodic reaction:

$$Al_2O_3 + 6e^- = 2Al + 3O^{2-} \qquad (9)$$

Total reaction:

$$3[C] + Al_2O_3 = 2Al + 3CO \qquad (10)$$
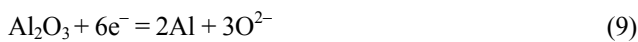
$$\Delta G = \Delta G^{\ominus} + RT \ln \frac{P_{CO}}{a_{[C]}}.$$

Thus, it can be seen that an increase of the carbon concentration in the hot metal leads to an increase of the [C] activity and a decrease of the electromotive force. Consequently, electrochemical etching is diminished as well as erosion of the refractory.

## 4. Conclusions

(1) The protective layer formed in the blast furnace hearth has a different phase assemblage under different operating conditions. When titanium ore is charged, the protective layer evolves into double layers, which are a tita-

*1024*

*Int. J. Miner. Metall. Mater., Vol. 22, No. 10, Oct. 2015*

nium-bearing layer and a graphite layer. The main phases in the titanium-bearing layer are Ti(C,N), slag, and iron, whereas the graphite phase layer mainly contains graphite and the slag phase.

(2) The main source of the slag phase in the protective layer is the coke ash. The evolution behavior of the coke ash was analyzed in combination with an investigation of the blow-down blast furnace. The main phase of the protective layer slag is magnesium melilite ($Ca_2MgSi_2O_7$), and the compounds of high melting point formed in the slag phase have a beneficial effect on the stability of the protective layer.

(3) The formation of the protective layer can be promoted by optimizing the composition of the coke ash. The main measures include reducing the $Al_2O_3$ content to promote the reduction of $SiO_2$, and increasing the content of CaO favorable towards the generation of the magnesium melilite phase. These measures are favorable to the formation of a viscous layer to protect the hearth.

(4) The aluminum phase generated in the protective layer is explained by the electrochemical corrosion theory in this paper. The erosion of refractory can be decreased by increasing the carbon concentration in the hot metal.

## Acknowledgements

## References

[1]   Z.J. Liu, J.L. Zhang, H.B. Zuo, and T.J. Yang, Recent progress on long service life design of Chinese blast furnace hearth, *ISIJ Int.*, 52(2012), No. 10, p. 1713.

[2]   S.R. Zhang, Ironmaking progress in Chinese, [in] *The 5th International Congress on the Science and Technology of Ironmaking*, Shanghai, 2009.

[3]   H.B. Luengen and P. Michael, Ironmaking progress in Western Europe, [in] *The 5th International Congress on the Science and Technology of Ironmaking*, Shanghai, 2009.

[4]   J. Li, Z.T. Zhang, L.L. Liu, W.L. Wang, and X.D. Wang, Influence of basicity and $TiO_2$ content on the precipitation behavior of the Ti-bearing blast furnace slags, *ISIJ Int.*, 53(2013), No. 10, p. 1696.

[5]   H.B. Zhao, S.S. Cheng, and M.G. Zhao, Analysis of all-carbon brick bottom and ceramic cup synthetic hearth bottom, *J. Iron Steel Res. Int.*, 14(2007), No. 2, p. 6.

[6]   R. Van Laar, E. Van Stein Callenfels, and M. Geerdes, Blast furnace hearth management for safe and long campaigns, *Iron Steelmaker*, 30(2003), No. 8, p. 123.

[7]   S.S. Cheng, T.J. Yang, Q.G. Xue, H.B. Zuo, X.W. Gao, and W.G. Yang, Numerical simulation for the lower shaft and the hearth bottom of blast furnace, *J. Univ. Technol. Beijing*, 10(2003), No. 3, p. 16.

[8]   X.F. Lei and X.X. Xue, Preparation, characterization and photocatalytic activity of sulfuric acid-modified titanium-bearing blast furnace slag, *Trans. Nonferrous Met. Soc. China*, 20(2010), No. 12, p. 2294.

[9]   C.H. Lin, W.T. Cheng, and S.W. Du, Numerical prediction on the variation of temperature in the eroded blast furnace hearth with titanium dioxide in hot metal, *Int. Commun. Heat Mass Transfer*, 36(2009), No. 4, p. 335.

[10]  L. Zhang, L.N. Zhang, M.Y. Wang, G.Q. Li, and Z.T. Sui, Recovery of titanium compounds from molten Ti-bearing blast furnace slag under the dynamic oxidation condition, *Miner. Eng.*, 20(2007), No. 7, p. 684.

[11]  R. Benesch, A. Lędzki, R. Kopeć, and R. Stachura, Investigations into titanium distribution between metal and slag in liquid phases, *Thermochim. Acta*, 152(1989), No. 2, p. 433.

[12]  C.L. Fan, H. He, K.H. Zhang, and S.C. Han, Structural developments of artificial graphite scraps in further graphitization and its relationships with discharge capacity, *Electrochim. Acta*, 75(2012), p. 311.

[13]  L.H. Zou, B.Y. Huang, Y. Huang, Q.Z. Huang, and C.A. Wang, An investigation of heterogeneity of the degree of graphitization in carbon–carbon composites, *Mater. Chem. Phys.*, 82(2003), No. 3, p. 654.

[14]  S. Gupta, D. French, R. Sakurovs, M. Grigore, H. Sun, T. Cham, T. Hilding, M. Hallin, B. Lindblom, and V. Sahajwalla, Minerals and iron-making reactions in blast furnaces, *Prog. Energy Combust. Sci.*, 34(2008), No. 2, p. 155.

[15]  S.T. Cham, V. Sahajwalla, and R. Sakurovs, The dissolution of cokes in molten iron, [in] *21th Annual International Pittsburgh Coal Conference*, Osaka, 2004.

[16]  J. Brännbacka and H. Saxén, Novel model for estimation of liquid levels in the blast furnace hearth, *Chem. Eng. Sci.*, 59(2004), No. 16, p. 3423.

[17]  X.Q. Wang, *Smelting of Vanadium and Titanium Magnetite in Blast Furnace*, Metallurgical Industry Press, Beijing, 1994.

[18]  K. Datta, P.K. Sen, and S.S. Gupta, Effect of titanium on the characteristics of blast furnace slags, *Steel Res.*, 64(1993), No. 5, p. 232.

[19]  Z.Y. Chen, X. Zhang, and D.G. Yang, Electrochemical corrosion of carbon-containing refractories, *J. Chin. Ceram. Soc.*, 15(1991), p. 442.